# Measuring Breathing Wall's Effectiveness and Dynamic Behaviour

Andrea Alongi[1], Adriana Angelotti[1,*], Livio Mazzarella[1]

[1]Politecnico di Milano, Energy Department, via Lambruschini 4, 20156 Milano, Italy

[*]Corresponding author: adriana.angelotti@polimi.it

## Abstract

Breathing Walls are building structures based on porous materials crossed by an airflow, acting both as building envelope and ventilation system components.

In climates where both heating and cooling needs are relevant, pro-flux configuration (heat and air mass both flowing in the same direction) might be alternated with contra-flux configuration (heat and air mass flowing in opposite directions) during the year or even the day. Understanding and modelling the Breathing Walls stationary and dynamic behaviour is thus fundamental, in order to optimize their design and fully exploit their energy saving potential.

To this purpose, in this experimental study a small scale no fines concrete Breathing Wall is investigated. The steady-state contra-flux tests performed in the DAVTB laboratory apparatus are used to derive the heat recovery efficiency of the sample as a function of the crossing airflow velocity. Effectiveness of this technology is then evaluated on a virtual case study, showing that an optimal airflow velocity across the Breathing Wall can be found, leading to energy savings between 9% and 14%. Dynamic tests, performed assuming a sinusoidal variation of the operative temperature on one side of the sample, show how airflow velocity affects the Breathing Wall inertia and dynamic behaviour.

## Keywords

Breathing Wall, Dynamic Insulation, heat recovery efficiency, experimental study, periodic boundary conditions

## Introduction

Breathing Wall technology has been studied since the past decades, being considered a promising technical solution to reduce building energy needs [1,2]. It is a building envelope technology based on the integration of air permeable walls and roofs into the ventilation plant: ventilation air crosses at low speed the porous layers of the envelope, therefore acting both as a heat exchanger and a filter. Considering the directions of heat flux and airflow, it is possible to define two main operating conditions: *pro-flux* if they happen in the same direction, *contra-flux* when they move in opposite direction. Most of the works in literature focus on the latter working condition, which is generally considered the most suitable for cold climates, since it allows to reduce the heat losses and pre-heat the ventilation air [3]. Moreover, when the airflow is directed inward, Breathing Walls also act as filters linked to the ventilation plant. As demonstrated in [3-5], this technology is able to achieve high level of filtration of PM10s with very limited pressure drop, thanks to the low airflow velocity typically used (lower than 0.01 m/s).

In turn, in climates where both heating and cooling needs are relevant, pro-flux and contra-flux configurations might be alternated during the year [6] or even the day.

As far as heat transfer is concerned, Breathing Wall behavior has been investigated from the theoretical standpoint both in steady and periodic conditions [2,7]. In previous works by the Authors, the steady state temperature distribution across a *no-fines* concrete Breathing Wall sample has been measured in contra-flux conditions by means of the laboratory apparatus Dual Air Vented Thermal Box [8,9]. The collected data have then been used to validate the steady state analytical model. Both the model and the experimental data imply that the temperature distribution across the section follows an exponential trend. In contra-flux winter conditions, the temperature gradient grows moving from outer to inner surface, and the conductive heat flux density changes accordingly.

As far as materials are concerned, the main requirement for Breathing Wall application is a good air permeability, due to a high level of interconnection between pores in the matrix. Most of the works that can be found in literature focuses on insulating materials, such as mineral wool or cellulose fiber [5,10-12]. However, pervious concrete, also known as *no-fines* concrete, has been studied in [8,9,13]: it consists of a concrete mixture without fine aggregates like small gravel and sand. This mix design leads to a high porosity (around 30%) with a good air permeability, that makes this material a suitable choice for Breathing Wall applications.

Design and operation strategies for an energy efficient application of Breathing Walls still need to be clarified. The present study represents a first step in this direction. In this paper, the steady state experimental data obtained by the DAVTB apparatus on a pervious concrete Breathing Wall sample are processed in order to estimate the overall performance of the component (both in terms of conductive heat losses and heat recovery efficiency) as a function of the airflow velocity crossing the sample. These results are subsequently used to evaluate the performance of the component under discussion in the context of a simple virtual room, with the main purpose of finding the optimal design criteria to achieve the lowest possible energy losses under given working conditions.

Finally, a new set of tests have been performed to assess the sample behavior when subjected to steady periodic conditions. Going more in detail, while one side is kept at constant temperature, the other is subjected to a sinusoidal thermal fluctuation. The most relevant data collected are presented in this paper and used to evaluate the effects of the airflow velocity on the inertial behavior of the Breathing Wall under investigation.

**Nomenclature**

| | | | |
|---|---|---|---|
| | | *Greek symbols* | |
| $c$ | specific heat [J/(kg·K)] | $\varepsilon$ | porosity [%] |
| $H$ | height [m] | $\lambda$ | thermal conductivity [W/(m·K)] |
| $L$ | length [m] | $\eta$ | heat recovery efficiency [%] |
| $\dot{m}$ | mass airflow rate [kg/s] | $\rho$ | density [kg/m$^3$] |
| $n$ | air change rate [h$^{-1}$] | | |
| $\dot{q}$ | heat flux density [W/m$^2$] | *Subscripts* | |
| $\dot{Q}$ | heat losses [W] | *a, air* | air referred quantity |
| $S$ | area [m$^2$] | *BW* | Breathing Wall referred quantity |
| $t$ | time [h] | *e* | outdoor referred quantity |
| $T$ | temperature [°C] | *i* | indoor referred quantity |
| $u$ | air velocity across the wall [m/s] | *trad* | traditional wall referred quantity |
| $V$ | volume [m$^3$] | *T* | transmission referred quantity |
| $\dot{V}$ | airflow rate [m$^3$/h] | *V* | ventilation referred quantity |

# Methods

The work presented in this paper is based on the application of experimental results to analytically investigate the performance of Breathing Walls through a virtual case study. Therefore, as a first step the performance of a no-fines concrete sample has been investigated at various airflow velocities. Then, the main results, such as surface temperature variations and heat recovery efficiency, have been used to evaluate the effect of this technology on the heat losses of a reference room. Moreover, experimental results on the same sample wall under steady periodic regime are presented for the first time and discussed.

*The experimental measurements*

Measurements were performed on a *no fines* concrete wall, using the Dual Air Vented Thermal Box (DAVTB) apparatus developed in the Building Physics Laboratory of the Energy Department at the Politecnico di Milano (Figure 1 and Figure 2). Both the sample and the experimental setup are thoroughly described in previous publications [8,9]. The DAVTB apparatus is based on: two insulated chambers (or boxes) divided by the sample (1 m x 1 m x 0.15 m wall in this work), a hydraulic plant (used to control operative temperature in both boxes separately and obtain the desired boundary conditions) and an air recirculation loop, which allows to control airflow velocity through the sample, both in verse and magnitude. In all tests the temperature distribution across the sample and the average airflow velocity were measured every 5 seconds.

With regard to thermal boundary conditions, tests can be divided in two groups. In the first one, steady-state boundary conditions were set on both sides of the sample (namely in both chambers), with operative temperature set points of 15 °C (outdoor) and 40 °C (indoor), to achieve a 25 °C temperature difference, typical for winter design conditions in Milan. This group of tests was already presented and discussed in [8,9] in the validation process for the analytical model presented in literature for steady state conditions, and its outcomes are used here to obtain surface temperatures and heat recovery efficiency of the sample Breathing Wall.

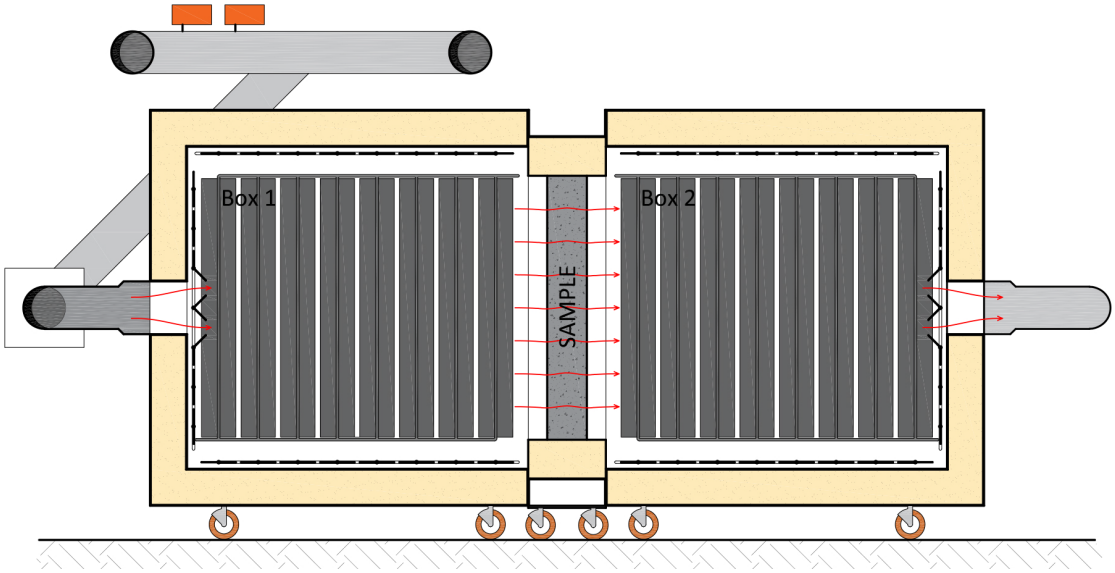


Figure 1. Vertical section of the DAVTB apparatus. The radiative panels are visible inside both Box 1 and 2, along with part of the air recirculation plant. The concrete sample between the chambers is also represented.

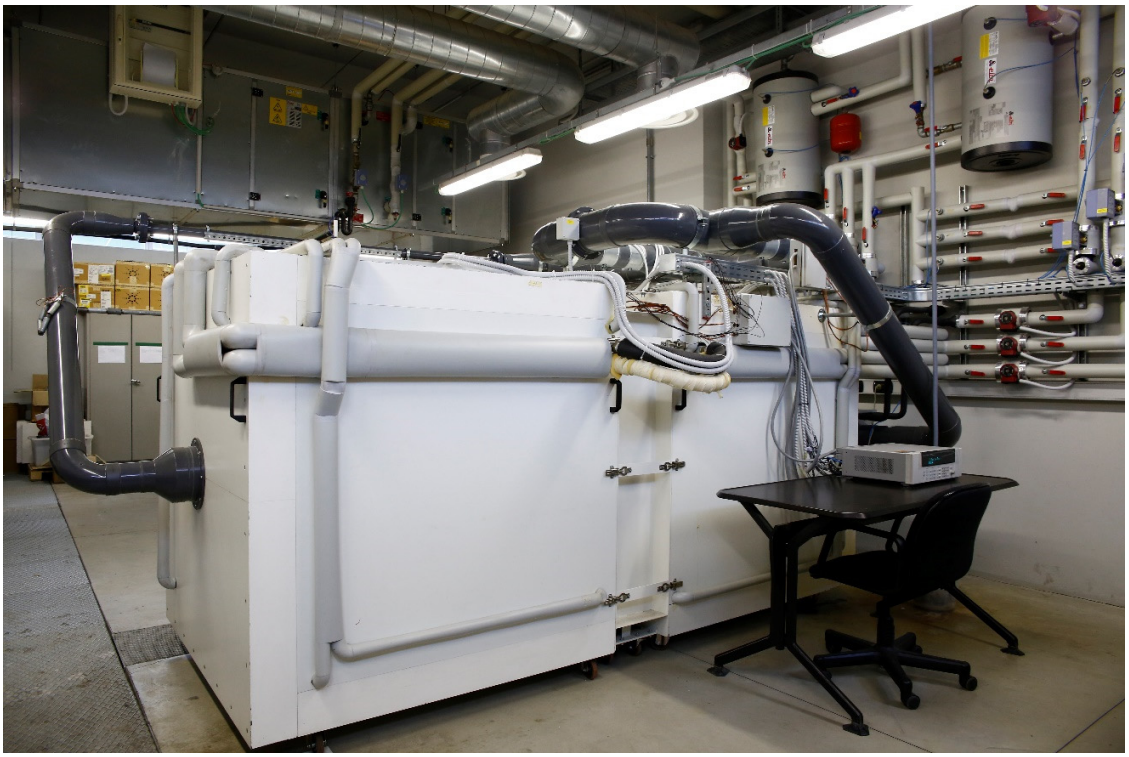

Figure 2. General picture of the DAVTB apparatus. Both chambers are visible on the foreground (Box 1 on the right and Box 2 on the left) with the metal frame bearing the sample in between. The hydraulic plant is displayed in the background (up right corner of the picture).

The second group of measurements featured a steady-periodic (sinusoidal) pattern on one side (average temperature 26 °C and amplitude 6 °C – i.e. simulating outdoor condition) and a steady-state condition on the other (26 °C – i.e. simulating indoor condition), to replicate summer boundary conditions in Milan.

Considering the airflow through the sample, in both groups five different average air velocities were assumed (0.001 m/s, 0.003 m/s, 0.006 m/s, 0.009 m/s and 0.012 m/s). Moreover, for both groups a reference test without airflow was performed to replicate the behavior of a traditional wall as a benchmark. In each test air flows from Box 1 (outdoor) to Box 2 (indoor). As a consequence, the steady-state tests are carried out in contra-flux condition, while the pro-flux and contra-flux conditions are alternated in the dynamic tests. The boundary conditions used in the various laboratory tests performed are summarized in Table 1.

Table 1. temperature and airflow velocity in the two groups of laboratory tests.

| | Box 1 | Box 2 |
|---|---|---|
| Temperature – steady state tests | 15 °C | 40 °C |
| temperature – steady periodic state tests | $T_{BOX1}(t) = 26 + 6\sin(\frac{2\pi t}{24})$ [°C] , t [h] | 26 °C |
| airflow velocity | 0 m/s, 0.001 m/s, 0.003 m/s, 0.006 m/s, 0.009 m/s, 0.012 m/s (from Box 1 to Box 2) | |

Finally, as far as the sample is concerned, it consists of a *no-fines* concrete slab 15 cm thick and 1 $m^2$ large. Its properties have been measured through a series of laboratory tests. First of all, its porosity $\varepsilon$ has been assessed to be equal to (30±2) % using the Archimedes method. Then, by combining volume and mass measurements, the density $\rho$ of the solid matrix has been calculated, obtaining (2483±87) kg/$m^3$. Finally, by applying the Transient Plane Source (TPS) technique [14] to dedicated samples, the values for specific heat capacity $c$ and thermal conductivity $\lambda$ of the solid matrix have been measured, respectively equal to (1013±157) J/(kg·K) and (1.76±0.08) W/(m·K). These values, combined with the corresponding thermos-physical properties of the air, have been used to calculate the quantities related to the overall porous medium, through the volume average method. Results are reported in Table 2: while porosity and thermal conductivity have already been verified in [8,9], the others will be discussed in a future work.

Table 2. thermos-physical properties of the *no-fines* concrete sample.

| quantity | value |
|---|---|
| porosity $\varepsilon$ | (30±2) % |
| density $\rho$ | (1738±61) kg/$m^3$ |
| specific heat capacity $c$ | (1011±110) J/(kg·K) |
| thermal conductivity $\lambda$ | (1.24±0.09) W/(m·K) |

*The virtual case study*

The energy saving potential of the experimentally investigated Breathing Wall was then assessed using a virtual case study in steady state conditions. It consists in a box-shaped room with a single external surface *S*, made of *no-fines* concrete, like the one experimentally investigated, while the rest of the envelope is assumed adiabatic. The external surface dimensions are 4 m x 3 m, and the room third dimension is assumed equal to 4 m, 6 m and 8 m alternatively, leading to three different volumes *V* and *S/V* ratios. Finally, a constant indoor-outdoor temperature difference of 25 °C and air change rate of 0.5 $h^{-1}$ were assumed. Data for the three cases are summarized in Table 3, while a simple representation is provided in Figure 3.

Table 3. Main data used in the calculations based on the reference room.

| | Case 1 | Case 2 | Case 3 |
|---|---|---|---|
| height *H* [m] | 3 | 3 | 3 |
| side $L_1$ [m] | 4 | 4 | 4 |
| side $L_2$ [m] | 4 | 6 | 8 |
| external envelope *S* [$m^2$] | 12 | 12 | 12 |
| volume *V* [$m^3$] | 48 | 72 | 96 |
| *S/V* [$m^{-1}$] | 0.250 | 0.167 | 0.125 |
| air change rate $n_V$ [$h^{-1}$] | 0.5 | 0.5 | 0.5 |
| airflow rate $\dot{V}$ [$m^3$/h] | 24 | 36 | 48 |
| temperature difference $\Delta T$ [°C] | 25 | 25 | 25 |

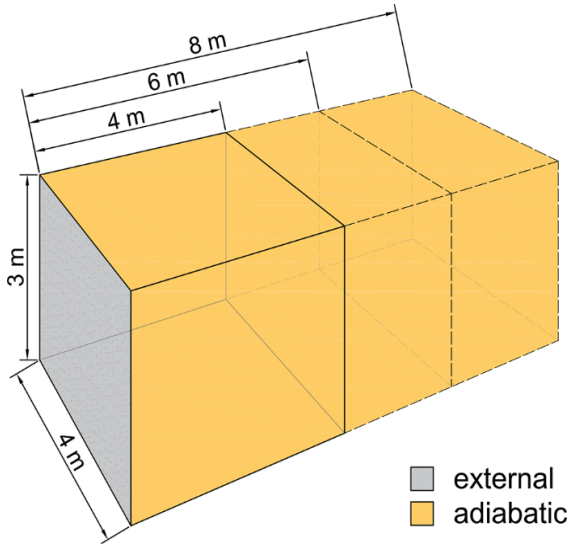


Figure 3. schematic representation of the virtual case study. The external wall (which is divided in an airtight and a Breathing Wall part) is represented in gray, while the adiabatic envelope is represented in yellow.

The case study was used in synergy with the outcomes of the steady state measurements illustrated before to calculate the overall heat losses. Going more in detail, they can be defined as:

$$\dot{Q}_L = \dot{Q}_T + \dot{Q}_V \quad (1)$$

where $\dot{Q}_T$ and $\dot{Q}_V$ are the conduction and ventilation losses respectively. Heat transfer through the external surface was calculated considering that part of it can work as a Breathing Wall ($S_{BW}$) and part as a traditional airtight one ($S_{trad}$). $\dot{Q}_L$ was calculated for increasing values of the average airflow velocity through the Breathing Wall up to 0.013 m/s, in order to identify the optimal working conditions. The airflow velocity was also used to evaluate the amount of external surface working as a Breathing Wall to meet the required air change rate. Therefore, since the external surface is:

$$S = \mathrm{S}_{BW} + \mathrm{S}_{trad}, \quad (2)$$

we can define the Breathing Wall area as

$$\mathrm{S}_{BW}(u) = min\left(\frac{\dot{V}}{u}; S\right), \quad (3)$$

where $\dot{V}$ is the required airflow rate and $u$ is the airflow velocity through the Breathing Wall. Whenever $u$ is too low to guarantee that the airflow through the Breathing Wall entirely covers the required airflow rate (i.e. $S_{BW} = S$), it is assumed that the missing airflow is provided by a traditional ventilation system (namely, without passing through the Breathing Wall).

Therefore, conduction heat losses are calculated as:

$$\dot{Q}_T = \mathrm{S}_{BW} \cdot \dot{q}_{T,BW} + \mathrm{S}_{trad} \cdot \dot{q}_{T,trad}, \quad (4)$$

where the subscript *BW* represents the Breathing Wall section of the envelope and *trad* represents the airtight one. The heat flux density at the inner surface is calculated using the suitable analytical model according to the working condition [2], as in the following equation:

$$\dot{q}_{T,i} = -\lambda \cdot \left.\frac{dT}{dx}\right|_i = \begin{cases} -\lambda \cdot \frac{T_L - T_0}{L} & \text{(traditional wall)} \\ -\lambda \cdot \frac{A \cdot (T_L - T_0)}{e^{AL} - 1} \cdot e^{AL} \quad A = \frac{\rho_{air} c_{p,air} u}{\lambda} & \text{(Breathing Wall)} \end{cases} \quad (5)$$

where $\lambda$ is the thermal conductivity of the wall, that is assumed to be made of *no fines* concrete in this analysis. Surface temperatures $T_L$ (indoor) and $T_0$ (outdoor) were calculated as a function of airflow velocity across the wall using a correlation based on the steady state measurements performed during the laboratory tests.

Ventilation heat losses are calculated as:

$$\dot{Q}_V = \dot{m}_{BW} \cdot c_{p,air} \cdot \eta_{BW} \cdot \left(T_{a,i} - T_{a,e}\right) + (\dot{m}_V - \dot{m}_{BW}) \cdot c_{p,air} \cdot \left(T_{a,i} - T_{a,e}\right) \quad (6)$$

where mass airflow is treated according to its path ($\dot{m}_{BW}$ if it crosses the Breathing Wall section or $\dot{m}_V - \dot{m}_{BW}$ if it is a complementary flow entering directly into the room), calculated as:

$$\dot{m}_{BW} = \mathrm{S}_{BW} \cdot u \cdot \rho_{air} \quad (7)$$

$$\dot{m}_V = n_V \cdot V \cdot \rho_{air} \qquad (8)$$

Moreover, according to Eq. (6), a heat recovery efficiency is considered for the airflow passing through the porous matrix of the *no fines* concrete wall, defined as:

$$\eta_{BW} = \frac{(T_L - T_{a,e})}{(T_{a,i} - T_{a,e})} \qquad (9)$$

where $T_L$ is the temperature of the inner surface of the wall, and $T_{a,e}$ and $T_{a,i}$ are the outdoor and indoor air temperature respectively. All their values are taken from the steady state measurements.

To summarize, according to the average airflow velocity across the permeable part of the external wall, it is possible to identify two possible configurations:

- in one case, when the airflow velocity is sufficiently high, the permeable part of the external surface can provide all the airflow required and an airtight portion of the external surface can be identified ($S_{BW} < S$);
- on the other end, when the air velocity is too low, all the external surface works as a Breathing Wall and an additional airflow supply is required to meet the expected air change ($S_{BW} = S$).

## Results and Discussion

As a first step data resulting from the steady state experimental tests were interpolated to obtain correlations to evaluate the superficial temperatures $T_L$ and $T_0$ and the heat recovery efficiency $\eta_{BW}$ as function of the specific airflow crossing the *no fines* concrete sample. Average experimental data (Table 4) have been used to derive polynomial interpolation such as:

$$f(x) = p_1 \cdot x^3 + p_2 \cdot x^2 + p_3 \cdot x + p_4 \qquad (10)$$

where $x$ is the air velocity normalized subtracting the mean (0.005185 m/s) and dividing by the standard deviation (0.004715 m/s). Coefficients $p_1$ to $p_4$ have been calculated using the Matlab® Curve Fitting Toolbox and are reported in Table 5.

The resulting curves are represented in Figure 4 and Figure 5. It is important to notice that the heat recovery efficiency of the airtight wall represents the ideal upper limit of $\eta_{BW}$, and was calculated using temperatures measured during the reference test at null airflow velocity. In the case of the no-fines concrete sample it is found $\eta_{BW}$ (u=0) = 72.4%.

Table 4. average surface temperatures and heat recovery efficiencies from experimental data.

| velocity | $T_0$ | $T_L$ | $\eta_{BW}$ |
|---|---|---|---|
| 0 (airtight) | 22.8 °C | 32.6 °C | 72.46% |

Table 5. polynomial interpolations coefficients for the surface temperatures and the heat recovery efficiency.

| coeff. | $T_0$ | $T_L$ | $\eta_{BW}$ |
|---|---|---|---|
| $p_1$ | -0.2147 °C | -0.2069 °C | -0.00753 |

| | | | |
|---|---|---|---|
| 0.001 m/s | 21.4 °C | 31.3 °C | 67.11% |
| 0.003 m/s | 19.9 °C | 29.5 °C | 60.02% |
| 0.006 m/s | 17.8 °C | 26.7 °C | 49.14% |
| 0.009 m/s | 16.6 °C | 24.9 °C | 42.09% |
| 0.012 m/s | 15.8 °C | 23.1 °C | 34.84% |

| | | | |
|---|---|---|---|
| $p_2$ | 0.9834 °C | 0.732 °C | 0.02868 |
| $p_3$ | -2.703 °C | -3.645 °C | -0.1441 |
| $p_4$ | 18.26 °C | 27.46 °C | 0.5208 |

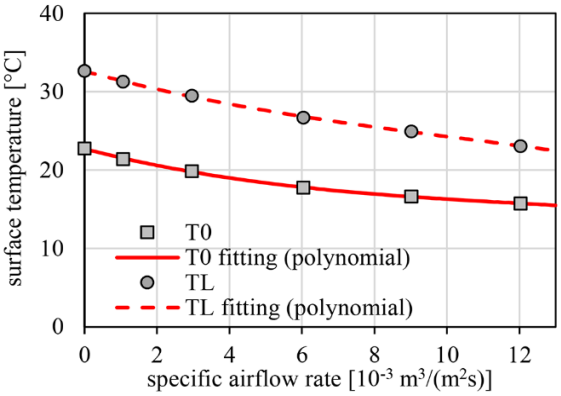


Figure 4. Measured indoor and outdoor surface temperatures vs specific airflow rate across the no fines concrete sample.

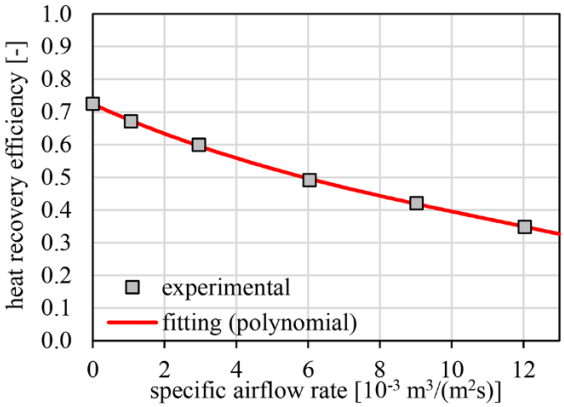


Figure 5. Heat recovery efficiency vs specific airflow rate across the no fines concrete sample.

Furthermore, $T_0$ and $T_L$ were used in Eq. (5) to calculate the conductive heat flux density through the external wall. The result is represented by the red line in Figure 6 and is compared with the experimental outcomes of the first tests group defined using the incremental ratio as:

$$\dot{q}_{T,exp} = -\lambda \cdot \frac{T_L - T_{L-\Delta x}}{\Delta x} \qquad (11)$$

where the $T_{L\_\Delta x}$ represents the measured temperature at a node located $\Delta x$ = 0.015 cm inward from the $L$ (indoor) surface. The agreement between experimental and analytical results is acceptable, also because the measurement errors (error bars in Figure 6) are relevant, due to the small temperature difference $T_L - T_{L-\Delta x}$.

The overall heat losses $\dot{Q}_L$ were then calculated for the three virtual rooms (case 1, 2 and 3), through the analytical procedure previously discussed. Results are represented in Figure 7, as a function of the average airflow rate through the air permeable section of the external wall, whose size changes according to Eq. (3). The decreasing part of each line is characterized by the requirement of an additional air supply, since the Breathing Wall airflow rate does not cover the whole need. Then, a minimum point representing the optimal solution can be observed. It is the smallest possible specific airflow through the Breathing Wall section that covers the overall demand without any additional contribution. In this way the heat recovery efficiency, that decreases when the specific airflow rate grows (Figure 5), is maximized. Also, the rise of conduction heat losses with respect to the null velocity (Figure 6) is low, since the deviation from linearity of the temperature distribution along the wall section is small: as explained in [1] and demonstrated in [8,9], when an air permeable wall is crossed by an airflow in *contra flux*

winter operating condition its temperature distribution grows exponentially from the outer to the inner surface. Moreover, its deviation from the linear distribution, which is typical in traditional wall under the same temperature boundary conditions, grows as the airflow velocity increases. Therefore, at relatively high speed, the conductive heat flux at the inner surface grows, as shown in Figure 6, while at lower velocity its value stays closer to the one obtained with no airflow, which is the ideal condition from the conduction stand point. The optimal specific airflow rate across the Breathing Wall is then 0.0006 $m^3/(m^2s)$, 0.0009 $m^3/(m^2s)$ and 0.0012 $m^3/(m^2s)$ for cases 1 to 3 and corresponds to an energy saving, compared to the traditional solution ($S_{BW} = 0\ m^2$, $u = 0\ m/s$) equal to 8.8 %, 11.8 % and 14.2 % respectively.

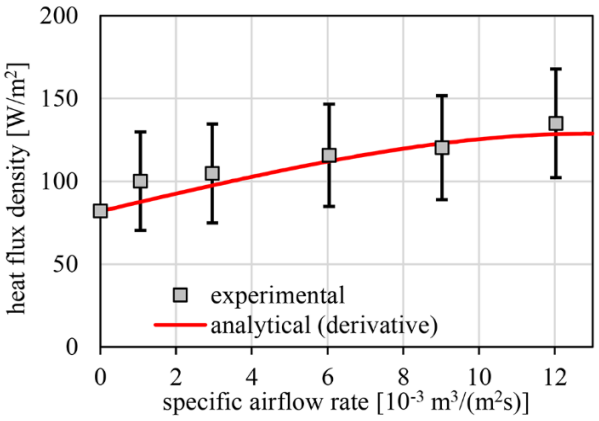


Figure 6. Conductive heat flux density vs specific airflow rate across the no fines concrete sample.

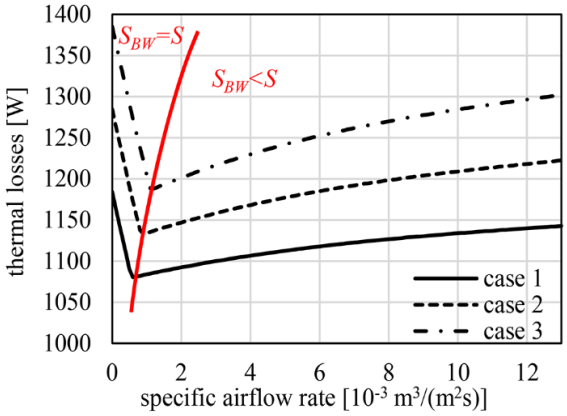


Figure 7. Overall heat vs specific airflow rate across the air permeable section of the external wall.

Considering now the second group of experimental tests, namely dynamic tests, Figure 8 compares the instantaneous boundary conditions (sinusoidal in Box 1 and constant in Box 2) to the average instantaneous surface temperature toward Box 2. Two main effects of the increasing airflow velocity through the sample can be observed: first of all, the time delay between the outdoor and inside surface peaks is reduced from 4.3 h (null velocity) to 3.0 h (maximum velocity). Secondly, the surface temperature pick amplitude grows from the 28 % (null velocity) to 56 % (maximum velocity) of the outdoor operative temperature one. Therefore, the increase in airflow velocity through the sample brings the indoor surface temperature closer to the outdoor boundary condition, namely reduces the sample thermal inertia. This is also demonstrated by Figure 9 representing the temperature distribution along the sample section, going from outside (x = 0 m – Box 1) to inside (x = 0.15 m – Box 2), during a 24 h period, for the airtight condition (top), for an average specific airflow rate condition (0.006 $m^3/(m^2s)$, middle), and for the maximum one (0.012 $m^3/(m^2s)$, bottom).

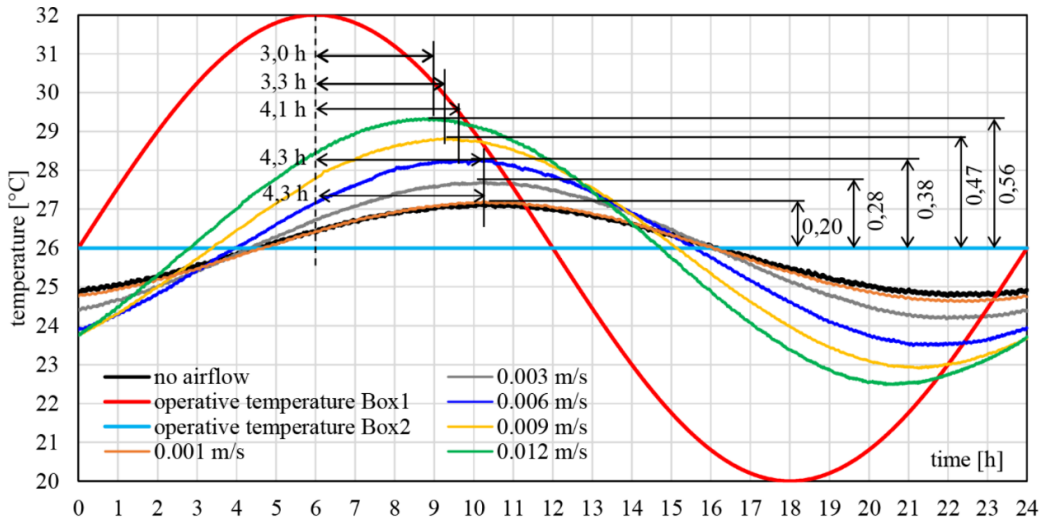


Figure 8. Comparison between boundary conditions and each internal surface temperatures measured.

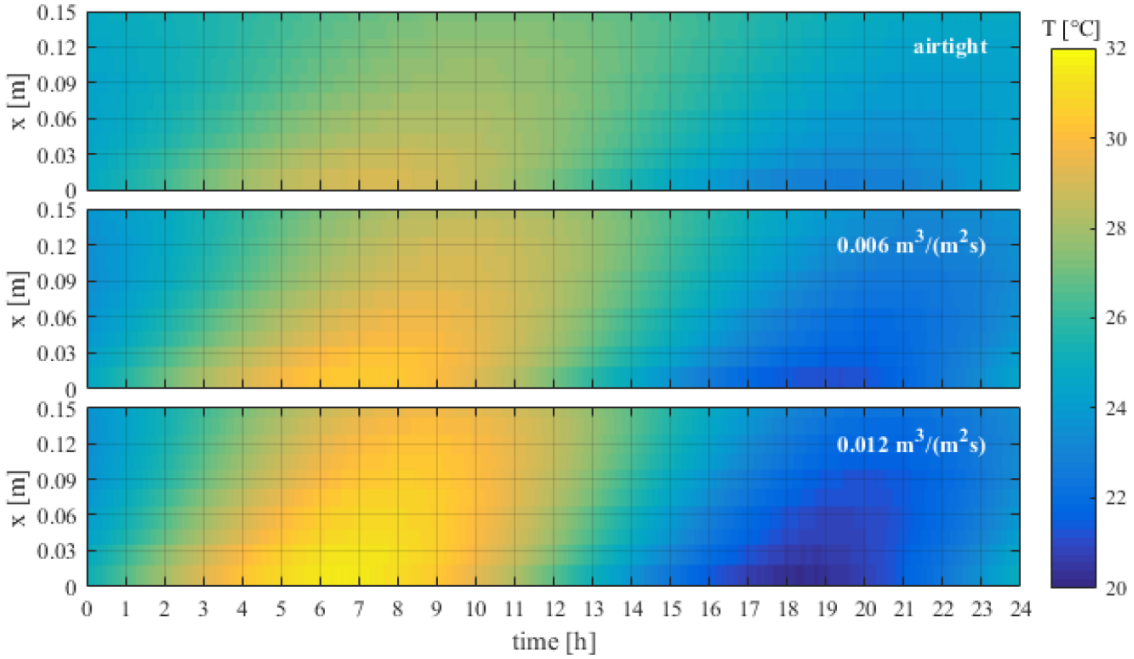


Figure 9. Temperature distribution along the section of the no fines concrete sample (x = 0 m facing Box 1 and x = 0.15 m facing Box 2) vs time.

The outcomes of this last analysis may provide useful indications for the application of Breathing Wall technology in practical conditions: in a real building, it might be possible to optimize hour by hour the airflow velocity and direction to minimize the overall thermal load on the conditioning plant, providing that the ventilation system is able to allow such a complex control on the airflow. In this way it would be possible to reduce conductive thermal load, while maximizing the energy recovered through the heat exchange. Moreover, it would be possible to optimize the amount of energy stored within the permeable envelope, according to the overall boundary conditions.

## Conclusions

Starting from the outcomes of steady state experimental tests on a Breathing Wall sample, the superficial temperatures on both sides and the heat recovery efficiency of the sample were correlated to the airflow velocity through it. These quantities were used to calculate the overall heat losses for a virtual case study, as a function of the velocity of the airflow crossing the Breathing Wall section of the only external surface (up to 0.013 m/s), and of the volume of the room investigated (case 1 to 3). The optimal condition is obtained when air moves with the lowest possible velocity able to provide all the airflow rate required, since it ensures the highest possible heat recovery efficiency, while minimizing the drop of insulating performance of the wall. In other terms, from the conductive point of view the deviation from the value obtained with an airtight envelope (which is the lowest possible) is minimal when the airflow velocity is low, while being high enough to completely cover the air change rate. At the same time, since the drop of the internal surface temperature is limited at low velocities, according to Eq. (9) and Figure 5 the heat recovery is maximized at these operating conditions.

The second set of experimental measurements shows the dynamic behaviour of the wall sample at various specific airflow rates: the increase of air velocity reduces both time delay (from 4.3 h down to 3. h) and attenuation (from 28 % up to 56 %) of the external thermal fluctuation.

These findings will be used in future works to address the heat recovery efficiency of *no fines* concrete Breathing Walls undergoing variable boundary conditions. Such investigation will potentially lead to a control strategy allowing to optimize the performance of the Breathing Wall, as both an envelope and a ventilation system component in a real context. As a matter of fact, the outcomes of the steady-periodic tests suggest that, in an implementation of this technology in a real building, it might be possible to optimize the control strategy for the ventilation plant in order to regulate the airflow velocity across the envelope and invert its direction (from outdoor to indoor and vice versa), minimizing the thermal load on the indoor conditioning plant according to both weather conditions and internal loads.

## Declaration

Andrea Alongi performed the experiments, analyzed the data, performed the calculations regarding the case study, discussed the results and prepared the manuscript. Adriana Angelotti conceived and designed the study, discussed the results and revised the manuscript. Livio Mazzarella discussed the results and revised the manuscript.

## References


1 Taylor BJ, Cawthorne DA and Imbabi MS. Analytical investigation of the steady-state behaviour of dynamic and diffusive building envelopes. Build Environ 1996; 31: 519-525.

2 Taylor BJ and Imbabi MS. The application of dynamic insulation in buildings. Renew Energ 1998; 15: 377-382.

3 Imbabi MS, Brown AR, Peacock A, et al. In: The transforming technology of dynamic breathing building, Proceedings Ecocity World Summit, San Francisco, USA, 2008, pp.1-12.

4 Taylor BJ, Webster R and Imbabi MS. The building envelope as an air filter. Build Environ 1999; 34: 353-361.

5 Di Giuseppe E, D'Orazio M and Di Perna C. Thermal and filtration performance assessment of a dynamic insulation system. Enrgy Proced 2015; 78: 513-518.

6 F. Ascione, N. Bianco, C. De Stasio, et al. Dynamic insulation of the building envelope: numerical modeling under transient conditions and
coupling with nocturnal free cooling, Appl. Therm. Eng. 84 (2015) 1-14.

7 Krarti M. Effect of air flow on heat transfer in walls. J Sol Energ-T Asme 1994; 116: 35-42.

8 Alongi A, Angelotti A and Mazzarella L. Experimental investigation of the steady state behaviour of Breathing Walls by means of a novel laboratory apparatus. Build Environ 2017; 123: 415-426.

9 Alongi A, Angelotti A and Mazzarella L. Analytical modelling of Breathing Walls: experimental verification by means of the Dual Air Vented Thermal Box lab facility. Energy Proced 2017; 140: 36-47.

10 Wang J, Du Q, Zhang C, et al. Mechanism and preliminary performance analysis of exhaust air insulation for building envelope wall. Energ Buildings 2018; 173: 516-529.

11 Dimoudi A, Androutsopoulos A and Lykoudis S. Experimental work on a linked, dynamic and ventilated, wall component. Energ Buildings 2004; 36: 443-453.

12 Baker PH. The thermal performance of a prototype dynamically insulated wall. Build Serv Eng Res T 2003; 24: 25-34.

13 Wong JM, Glasser FP and Imbabi MS, Evaluation of thermal conductivity in air permeable concrete for dynamic breathing wall construction. Cement Concrete Comp 2007; 29: 647-655.

14 He Y. Rapid thermal conductivity measurement with a hot disk sensor - part 1. Theoretical considerations. Thermochim Acta 2005; 436: 122-129.